Archives of Biochemistry and Biophysics 526 (2012) 44–53

Contents lists available at SciVerse ScienceDirect

Archives of Biochemistry and Biophysics

journal homepage: www.elsevier.com/locate/yabbi

Stability and binding of the phosphorylated species of the N-terminal domain of enzyme I and the histidine phosphocarrier protein from the *Streptomyces coelicolor* phosphoenolpyruvate:sugar phosphotransferase system

Rosa Doménech [a], Ana Isabel Martínez-Gómez [b], David Aguado-Llera [a], Sergio Martínez-Rodríguez [b], Josefa María Clemente-Jiménez [b], Adrián Velázquez-Campoy [c,d,e,*], José L. Neira [a,c,*]

[a] Instituto de Biología Molecular y Celular, Universidad Miguel Hernández, Elche (Alicante), Spain
[b] Departamento de Química-Física, Bioquímica y Química Inorgánica, Universidad de Almería, Almería, Spain
[c] Instituto de Biocomputación y Física de Sistemas Complejos, Unidad Asociada IQFR-CSIC-BIFI, Universidad de Zaragoza, Zaragoza, Spain
[d] Fundación ARAID, Diputación General de Aragón, Zaragoza, Spain
[e] Departamento de Bioquímica y Biología Molecular y Celular, Universidad de Zaragoza, Zaragoza, Spain

ARTICLE INFO

Article history:
Received 16 May 2012
and in revised form 6 July 2012
Available online 15 July 2012

Keywords:
Protein folding
Fluorescence
Protein stability
Isothermal titration calorimetry
Circular dichroism
NMR

ABSTRACT

The phosphotransferase system (PTS) is involved in the use of carbon sources in bacteria. It is formed by two general proteins: enzyme I (EI) and the histidine phosphocarrier (HPr), and various sugar-specific permeases. EI is formed by two domains, with the N-terminal domain (EIN) being responsible for the binding to HPr. In low-G + C Gram-positive bacteria, HPr becomes phosphorylated not only by phosphoenolpyruvate (PEP) at the active-site histidine, but also by ATP at a serine. In this work, we have characterized: (i) the stability and binding affinities between the active-site-histidine phosphorylated species of HPr and the EIN from *Streptomyces coelicolor*; and (ii) the stability and binding affinities of the species involving the phosphorylation at the regulatory serine of HPr^{sc}. Our results show that the phosphorylated active-site species of both proteins are less stable than the unphosphorylated counterparts. Conversely, the Hpr-S47D, which mimics phosphorylation at the regulatory serine, is more stable than wild-type HPr^{sc} due to helical N-capping effects, as suggested by the modeled structure of the protein. Binding among the phosphorylated and unphosphorylated species is always entropically driven, but the affinity and the enthalpy vary widely.

Introduction

The bacterial phosphoenolpyruvate:sugar phosphotransferase system modulates the use of carbon sources in bacteria. It is involved in: (i) transport and the uptake of several carbohydrates through the cell wall; (ii) cell movement towards these carbon sources (chemotaxis); and (iii) regulation of other metabolic pathways in both Gram-negative and Gram-positive bacteria [1–4]. The basic composition of the PTS is similar in all species described so far; it is formed by a cascade of phosphoryl-transfer steps from PEP to the sugar-specific enzyme II permeases (EIIs). The first two proteins in the cascade are common to all PTS substrates (the so-called "general PTS proteins"): the phosphocarrier proteins enzyme I and HPr. In the first step of the PTS, EI is phosphorylated by PEP, in the presence of Mg^{2+}, on the $N^{\varepsilon 2}$ atom of the active-site histidine; subsequently, the phosphoryl group is transferred to HPr, at the $N^{\delta 1}$ atom of its active-site histidine [2,5]; HPr is able to transfer the phosphate to the active site of an EII permease (usually, but not exclusively, at a histidine residue). In low-G + C Gram-positive bacteria and a few Gram-negative organisms, HPr can be also phosphorylated by an ATP-dependent kinase on a serine residue.

Sequence comparisons among several EIs and HPrs reveal significant identity [6]. The 64 kDa EI protein in the species described so far is a homodimer, whose self-association affinity is larger in the phosphorylated state than in the unphosphorylated one [7,8]. Limited proteolysis of EI^{ec}, with several proteolytic enzymes, yields two domains [9]. The EI N-terminal domain comprises, roughly, the first 230 residues of the protein; EIN contains the HPr-binding region and the active-site histidine [5]. The second C-terminal domain mediates dimerization and binds PEP in the presence of Mg^{2+} [10,11]. The structure of EIN has been determined by X-ray and NMR [12,13], and its complex with HPr has been characterized

* Corresponding authors. Address: Institute of Biocomputation and Physics of Complex Systems (BIFI), Universidad de Zaragoza, Zaragoza, Spain. Fax: +34 976762990 (A. Velázquez-Campoy); Instituto de Biología Molecular y Celular, Universidad Miguel Hernández, Avda. del Ferrocarril s/n, 03202 Elche (Alicante), Spain. Fax: +34 966658758 (J.L. Neira).
E-mail addresses: adrianvc@unizar.es (A. Velázquez-Campoy), jlneira@umh.es (J.L. Neira).

0003-9861/$ - see front matter © 2012 Elsevier Inc. All rights reserved.
http://dx.doi.org/10.1016/j.abb.2012.07.004

by NMR techniques [14]. The isolated EIN, which consists of an α-helical region (where HPr binds) and an α/β domain, is structurally similar to the phospho-histidine domain of the pyruvate-phosphate dikinase [15]. The structure of EIC is an $(\alpha/\beta)_8$ barrel, similar to the PEP-binding domain of PPDK [15].

Streptomyces is a soil-dwelling Gram-positive actinomycete, with a high G + C content, that grows on a variety of carbon sources. The complete genome of *Streptomyces coelicolor* has been sequenced, and the different components of the PTS have been reported [16–18]. We have undertaken an extensive description of the structures and conformational stabilities of the HPr^{sc} and EI^{sc} proteins as a first step to understand their binding reaction [19–22]. The binding of EI^{sc} and HPr^{sc} is enthalpically driven, whereas in other species is entropy-driven [23]; furthermore, the value of the K_D for the EI^{sc}–HPr^{sc} complex is larger (~100 μM) than those measured in *Escherichia coli* (9 μM) or *Mycoplasma capricolum* (7 μM) [10,24]. Therefore, it is necessary to understand the structural determinants responsible for those differences, specifically in the HPr binding region of EI^{sc} (that is, in EIN^{sc}).

In this work, we characterized: (i) the stabilities and the binding affinities of active-site and serine-regulatory phosphomimetics; and (ii) those parameters of the self active-site phosphorylated species for the EIN^{sc} and HPr^{sc}. Our results show that the phosphorylated active-site species of both proteins are less stable than the unphosphorylated ones, probably due to disruption of hydrogen-bonds occurring upon phosphorylation. On the other hand, HprS47D is more stable than wild-type HPr^{sc} due to helical N-capping effects, as suggested by its position in the modeled structure [25]. The binding reactions among the phosphorylated or the unphosphorylated species are always entropically driven, but the affinity and the binding enthalpy vary among the reactions. The changes in the thermodynamic parameters suggest small conformational rearrangements around the corresponding active sites upon binding.

Materials and methods, and experimental procedures

Materials

Deuterium oxide and deuterated-Tris were obtained from Apollo Scientific (Stockport, UK), and TSP was from Sigma (Barcelona, Spain). The Ni^{2+} resin was from GE Healthcare (Barcelona, Spain). Dialysis tubing (Spectra Por), with a molecular weight cut-off of 3500 Da, was from Spectrum Laboratories (Japan). Standard suppliers were used for all other chemicals. Water was deionized and purified on a Millipore system.

Protein expression and purification

To mimic the phosphorylated state of EIN^{sc}, the active-site His186 of EIN^{sc} was mutated to Asp (EINH186D) by using the QuikChange site-directed mutagenesis kit (Agilent, Spain), following the instructions of the manufacturer. Oligonucleotides were synthesized by Invitrogen (Spain). Mutations were verified by DNA sequencing (Secugen, Spain). The mutated plasmid was introduced into an *E. coli* C41 strain [26] and the cells were grown in LB medium. Purification of EINH186D was similar to that of wild-type EIN^{sc} [27]. Intact EI^{sc} was produced and purified as described [21].

The P∼HPr^{sc} was mimicked by mutation of the active site histidine, His15 to Asp; the Ser47 was also mutated to Asp to mimic the (P∼Ser)HPr^{sc}. The mutagenesis protocol was the same used for the EINH186D mutant. Expression and purification of HPr^{sc} variants were the same as for wild-type [19].

The ^{15}N-labeled proteins (wild-type HPr^{sc} and EIN^{sc}) were prepared by growing the C41 cells in M9 minimal medium, containing $^{15}NH_4Cl$ (Sigma–Aldrich, Spain) as the sole ^{15}N source, as described [28]. Protein concentrations were determined from the absorbance of individual amino acids [29] at 280 nm, by using a Shidmazu UV-1601 spectrophotometer (Japan), in a 1-cm-path-length cell (Hellma).

Protein phosphorylation

To keep wild-type HPr^{sc} or EIN^{sc} fully phosphorylated during the experiments, we followed two protocols:

Phosphorylation of wild-type EIN^{sc}

Phosphorylation of wild-type EIN^{sc} was prepared in a reaction mixture (500 μl), containing 300 μM of uniformly (>99%) ^{15}N-labeled protein (for NMR experiments), or 300 μM of unlabelled protein (for the CD[1] and fluorescence experiments), 1 μM HPr^{sc}, 10 μM of EI^{sc}, 5 mM $MgCl_2$, 5 mM DTT and 20 mM PEP, at the desired pH. Under these conditions, EIN^{sc} remained fully phosphorylated for at least 12 h at 25 °C, as judged from the NMR experiments.

Phosphorylation of wild-type HPr^{sc}

Phosphorylation of wild-type HPr^{sc} was prepared in a reaction mixture (500 μl), containing 300 μM of uniformly (>99%) ^{15}N-labeled protein (for the NMR experiments), or 300 μM of unlabelled protein (for the CD and fluorescence experiments), 10 μM of EI^{sc}, 5 mM $MgCl_2$, 5 mM DTT and 20 mM PEP, at the desired pH. Under these conditions, HPr^{sc} remained fully phosphorylated for at least 12 h at 25 °C, as judged from the NMR experiments.

To be sure that phosphorylation in wild-type HPr^{sc} had taken place, control experiments were carried out with no PEP added to the mixture reaction. In these control experiments no changes were observed for the chemical shifts of the active-site histidine, when compared to those measured in aqueous solution, as measured by HMQC experiments (see 'NMR spectroscopy'). Control experiments were also carried out by acquiring the CD spectra of the samples (see 'Results').

Fluorescence

Spectra were collected on a Cary Eclipse spectrofluorometer (Varian, California, USA) interfaced with a Peltier system. A 1-cm path-length quartz cell (Hellma) was used. Experiments were performed with a final protein concentration of 20 μM in Tris buffer, pH 7.0 (50 mM); for the measurements with the phosphorylated samples, the solutions of unlabelled wild-type HPr^{sc} or EIN^{sc} were diluted appropriately.

Steady-state fluorescence measurements

Spectra were acquired by excitation either at 280 (for wild-type EIN^{sc} and EINH186D, which lack tryptophan residues) or 295 nm (for HPr^{sc} and its mutants, with a single tryptophan). The fluores-

[1] *Abbreviations used:* CD, circular dichroism; DSC, differential scanning calorimetry; EI, enzyme I; EI^{sc}, the EI from *Streptomyces coelicolor*; EIC, the C-terminal region of EI (comprising approximately the last 300 residues); EIC^{sc}, the C-terminal region of EI^{sc}; EIN, the N-terminal region of EI (comprising approximately the first 250 residues); EIN^{sc}, the N-terminal domain (residues 1-246) of EI^{sc}; EIN^{ec}, the N-terminal domain of EI from *E. coli*; EII, enzyme II permease; HMQC, heteronuclear multiple quantum coherence; HPr, histidine-phosphocarrier protein; HPr^{sc}, the HPr from *Streptomyces coelicolor*; HPr^{bs}, the HPr from *Bacillus subtilis*; HPr^{ec}, the HPr from *Escherichia coli*; ITC, isothermal titration calorimetry; K_D, dissociation constant; P∼EI, phosphorylated EI species at the active-site histidine; P∼EIN^{sc}, phosphorylated EIN^{sc} species at the active-site histidine (H186); P∼HPr^{sc}, phosphorylated HPr^{sc} species at the active-site histidine (H15); (P∼Ser)HPr^{sc}, phosphorylated HPr^{sc} species at the regulatory serine (S47); PEP, phosphoenolpyruvate; PPDK, pyruvate phosphate dikinase; PTS, PEP-dependent phosphotransferase system; TSP, sodium trimethylsilyl-[2,2,3,3-$^2H_4$]-propionate; T_m, thermal-denaturation midpoint of an unfolding reaction (expressed in °C); UV, ultraviolet.

cence emission was collected between 300 and 400 nm. The excitation and emission slits were set to 5 nm. The spectrum of EINH186D species had a maximum at 305 nm as that of wild-type EIN^{sc} [27]; on the other hand, spectra for both HPr^{sc} mutants had a maximum at 333 nm, as in wild-type [19].

Thermal denaturations

Thermal denaturations were only carried out with the HPr proteins, due to the low fluorescence intensity observed in EIN^{sc} [27]. Excitation was carried out at 280 nm, and fluorescence emission was collected at 315, 335, and 350 nm; the scan rate was 60 °C h^{-1}, and the data were acquired every 0.2 °C.

Circular dichroism

Spectra were collected on a Jasco J810 (Japan) spectropolarimeter fitted with a thermostated cell holder and interfaced with a Peltier unit. The instrument was periodically calibrated with (+) 10-camphorsulphonic acid. Experiments were carried out in 0.1-cm path-length cells (Hellma) with a protein concentration of 20 μM, in Tris buffer, pH 7.0 (50 mM). For the experiments with the phosphorylated samples, the 300 μM protein solutions of unlabelled wild-type HPr^{sc} or EIN^{sc} were diluted appropriately.

Steady-state measurements

Spectra were acquired in the far-UV CD with a response time of 1 s and averaged over six scans, with a scan speed of 50 nm/min. The step resolution was 0.2 nm, and the bandwidth was 1 nm. Experiments were also attempted in the near-UV (with an 0.5-cm path-length cell, and 60 μM of protein), but the near-UV spectra of both wild-type HPr^{sc} and EIN^{sc} were very weak (even in P∼HPr^{sc} and P∼EIN^{sc}) due to the small number of aromatic residues [19,27].

Thermal denaturations

Thermal denaturations were performed at a constant heating rate of 60 °C h^{-1}, a response time of 8 s and acquiring data every 0.2 °C. Thermal scans were collected in the far-UV region at 222 nm from 25 to 95 °C. The experiments were repeated twice in two independent sets. Samples were transparent and no precipitation was observed after the heating; furthermore, the steady-state spectra for each protein after cooling to 25 °C were identical to those obtained before heating. In addition, the monitored voltages of the photomultiplier tube during the thermal scans did not show any sigmoidal behavior, but rather they increased linearly as the temperature was raised, suggesting reversibility of the transitions [30].

Thermodynamic parameters of the unfolding reactions were obtained by following the change in the physical property, Y (the fluorescence intensity or the ellipticity), according to:

$$Y = (Y_N + Y_D e^{(-\Delta G/RT)})/1 + e^{(-\Delta G/RT)}, \quad (1)$$

where $Y_N = \alpha_N + \beta_N[T]$ and $Y_D = \alpha_D + \beta_D[T]$ are the baselines of the folded and unfolded states, respectively, for which a linear relationship with temperature is assumed; R is the gas constant; and T is the temperature in K. The change in free energy, ΔG, is given by:

$$\Delta G(T) = \Delta H_m(1 - T/T_m) - \Delta C_p[(T_m - T) + T \ln T/T_m)], \quad (2)$$

where ΔH_m is the van't Hoff unfolding enthalpy; T_m is the midpoint of the thermal denaturation (in K); and ΔC_p is the heat capacity change of the folding reaction. The shape of Eq. (2) (with exponential terms above and below the rate) does not impose restrictions on the value of the ΔC_p; thus, fitting of the experimental data and the exact determination of the T_m (which is the thermodynamic parameter used for a comparison of stability among the assayed species) do not rely on a pre-fixed value of the ΔC_p. Attempts to determine two transitions from the thermal denaturations of phosphorylated species followed by fluorescence or CD (where two populations, un- and phosphorylated, are always observed, Fig. 4, Supplementary information) failed, since the fittings always resulted in the same two T_ms.

Fittings to Eqs. (1) and (2) were carried out by using the general curve-fit option of Kaleidagraph (Abelbeck software) running on a PC computer.

Differential scanning calorimetry

DSC experiments were carried out with a VP-DSC calorimeter (MicroCal, Northampton, MA). EIN^{sc} and EINH186D solutions were prepared by dialysis against the working buffer (10 mM MES, pH 6.5, and 200 mM NaCl) at 4 °C; lyophilized wild-type HPr^{sc}, Hpr-H15D and Hpr-S47D were dissolved in 10 mM phosphate buffer, pH 7.5. Assays with the P∼EIN^{sc} and P∼HPr^{sc} species were carried out by dissolving the wild-type EIN^{sc} and HPr^{sc} in the corresponding phosphorylation buffer (see 'Protein phosphorylation') in 10 mM Tris buffer, pH 7.5.

Calorimetric experiments were performed at a protein concentration of 90 μM, for the wild-type HPr^{sc} and EIN^{sc}, EINH186D proteins, and 60 μM for the HPr phosphomimetics. To minimize the amount of gas dissolved in the solution, the samples were degassed for 10 min at room temperature with gentle stirring before being loaded into the calorimetric cells. Samples were heated at a constant scan rate of 60 °C h^{-1} and held under an overpressure of 2 bars (28 psi) to avoid both bubble formation and evaporation at high temperatures. Buffer–buffer scans were performed to ensure proper instrument equilibration. To correct for small mismatches between the two cells, an instrumental baseline (i.e., buffer–buffer baseline) was subtracted from the protein endotherm before data analysis. All traces were dynamically corrected to account for the time-delayed response of the detector to the heat event that evolved within the calorimetric cell. After normalizing to protein concentration, a chemical baseline calculated from the progress of the unfolding transition was subtracted. Fitting of the endotherms was carried out by using the Origin 7.0 package supplied with the instrument.

Isothermal titration calorimetry

ITC measurements were performed by using a VP-ITC calorimeter (MicroCal, Northampton, MA). In all the assays, the sample cell (1.4 ml) was loaded with either EIN^{sc} or EINH186D (at a concentration of 15 μM); the syringe was loaded with either wild-type HPr^{sc} or the corresponding phosphomimetic species (at a concentration of 400 μM). For titrations involving the P∼EIN^{sc} and P∼HPr^{sc}, 150 μM of EIN^{sc} and 1.5 mM of HPr^{sc} were dissolved in the corresponding phosphorylation buffer (see 'Protein phosphorylation'), and loaded, respectively, into the cell and the syringe. As a control experiment, the individual dilution heats for P∼HPr^{sc} were determined by carrying out identical injections of the protein into the sample cell in the absence of wild-type EIN^{sc}. Control experiments to determine the dilution heats of HPr^{sc} have been described elsewhere [23].

A total of 28 injections of 10 μl were added sequentially to the sample cell after 400–800 s spacing to ensure that the thermal power returned to the baseline before the next injection. The amount of power required to maintain the reaction cell at constant temperature after each injection was monitored as a function of time. The isotherms (heat associated to each injection *versus* molar ratio of the reactants in the cell) were fitted to a single-site model assuming that the complex had a 1:1 stoichiometry. Data were

analyzed with software developed in our laboratories, implemented in the software package Origin 7.0 (OriginLab).

The ITC experiments were carried out in two buffers to analyze the contribution of the buffer ionization enthalpy: (a) 10 mM Tris, pH 7.0; and, (b) 10 mM Mops, pH 7.0 at 25 °C. Then, the apparent binding enthalpy change ($\Delta H_{meas;buffer}$) in the corresponding buffer is:

$$\Delta H_{meas;buffer} = \Delta H^0 + n_H \Delta H_{ion}, \quad (3)$$

where ΔH^0 is the buffer-independent binding enthalpy; ΔH_{ion} is the ionization enthalpy of the buffer; and n_H is the number of exchanged protons between the complex and the solvent during the binding reaction. ΔH^0 and n_H can be determined from linear regression by performing titration experiments in buffers with different ionization enthalpies.

NMR spectroscopy

The NMR data were acquired at 25 °C on a Bruker Avance DRX-500 spectrometer (Bruker GmbH, Germany), equipped with a triple resonance probe and z-pulse field gradients. Processing of spectra was carried out with the XWINNMR software.

1D-NMR experiments

TSP was used as the external chemical shift reference in the 1D-NMR spectra. Water was suppressed with the WATERGATE sequence [31]. Usually, 512 scans were acquired with a spectral width of 12 ppm, with 16 K data points in the time domain. The data matrix was zero filled to 32 K during processing. Experiments were carried out at pH 7.0 (50 mM phosphate buffer) at a final concentration of 50 mM); the lyophilized samples (HPr^{sc}, EIN^{sc} and its mutants) were dissolved in 90% H_2O/10% D_2O. Protein concentration was 100 μM.

We also acquired ^1H 1D-NMR spectra in 100% D_2O between pH 4.25 and 7.5 to follow the pH titration of the His15 in wild-type HPr^{sc} at a concentration of 80 μM (buffer concentration 50 mM). In these experiments we follow the changes in chemical shifts of $H^{\varepsilon 1}$ and $H^{\delta 2}$ protons, upon pH titration of the protons directly attached to the $N^{\delta 1}$ and $N^{\varepsilon 2}$. Sample cloudiness was observed at pHs below 4.75, and then caution should be taken with the acidic points. Precipitation and aggregation have been observed at these low pHs, and they have been attributed to complex titration of several aspartic and glutamic residues [19]. We also tried to determine the titration of the active-site histidine of His186 in EIN^{sc}, but since there are three imidazole rings in the protein, there was severe signal overlapping. Furthermore, the signals of His186 in the ^1H 1D-NMR spectra of P∼EIN^{sc} could not be followed due to the broadening of its $H^{\varepsilon 1}$ and $H^{\delta 2}$ protons; similar broadening of signals of $H^{\varepsilon 1}$ and $H^{\delta 2}$ protons have been shown in other imidazole rings, which have some of their protons hydrogen-bonded [32].

^1H–^{15}N-HMQC spectra

Two-dimensional ^1H–^{15}N-HMQC spectra [33] of wild-type HPr^{sc} and EIN^{sc} were acquired in D_2O at pH values ranging from pH 5.0 to 9.4, in the absence or in the presence of the corresponding phosphorylation buffer (see 'Protein phosphorylation'). Protein concentration was 300 μM. Removal of the residual water signal was achieved with presaturation. The delay during which ^{15}N and ^1H signals become antiphase was set to 22 ms to allow for refocusing of the magnetization coming from the $^1J_{NH}$ couplings. The ^1H transmitter was set to 4.80 ppm and the ^{15}N carrier to 210 ppm. Spectra were acquired with 2 K data points (in the F2 dimension) and 128 complex points (in the F1 dimension); usually, 96 scans *per* experiment were acquired. Spectral widths were 12 and 60 ppm for the ^1H- and the ^{15}N-dimensions, respectively; the States-TPPI method was used to achieve quadrature detection in the t_1 dimension [34]. Data were zero-filled to a 2 × 1 K matrix, in the direct and indirect dimensions, respectively, and processed by using sine square windows. Spectra were referenced according to Wishart et al. using TSP as internal reference at any of the different explored pHs [35]. Since all the measurements were carried out in D_2O, the readings from the pHmeter were corrected by adding 0.4 units. The chemical shifts of TSP are also pH-dependent, going from −0.015 at pH 7 to 0.003 at pH 3 [35]; we, therefore, interpolated or extrapolate to our current pH measurements by using a linear regression between those values.

The titration curves were fitted to the Henderson–Hasselbalch equation:

$$\delta = (\delta_a + \delta_b 10^{(pK_a - pH)})/(1 + 10^{(pK_a - pH)}), \quad (4)$$

where δ is the measured chemical shift for a particular pH; δ_a is the chemical shift of the species at low pH; δ_b is the chemical shift of the species populated at high pH; and pK_a is the titration midpoint of the acid–basic transition of the observed nuclei of the histidine ring.

Results

Structural features and stability of the HPr^{sc} phosphomimetic mutants and the P∼HPr^{sc} species

Phosphomimetic mutants

The far-UV CD spectra of wild-type HPr^{sc} and its mutants were identical (Fig. 1A), suggesting that the α + β structure of the protein was not changed. Furthermore, the methyl regions of the ^1H 1D-NMR spectra suggest that the mutants are native-like. Small changes were only observed for some methyl groups of Hpr-H15D (Fig. 1B); these changes were probably due to the removal of the imidazole side chain, and its ring-current shifts, which are affecting the methyl groups of the nearby Leu14 [36].

We carried out the stability measurements of the mutants at physiological pHs because of: (i) the comparison with data in the literature for other PTS proteins; and, (ii) the fact that stability of the wild-type HPr^{sc} remains constant between pH 7.0 and 9.0, but it decreases abruptly below or above those limits [19]. The T_m of Hpr-H15D, either measured by far-UV CD or fluorescence, was smaller than that of the wild-type (Table 1). The T_m of Hpr-S47D was larger than that of wild-type (Table 1 and Fig. 2A). We carried out the measurements with both HPr mutants at 90 and 60 μM (Fig. 1, SI), since at the highest concentration they precipitated; however, wild-type HPr^{sc} at the high concentration did not show evidence of aggregation during the DSC experiments ([19] and Fig. 4A, SI). At the low protein concentration, the samples did not show evidence of aggregation. Possibly, aggregation is due to features of the denatured states of both mutants. The values of the midpoints of the thermograms are in fair agreement with those reported by the other spectroscopic techniques (Table 1).

As the pH was increased, the chemical shifts of the $N^{\varepsilon 2}$ of His15 changed from 176 to 185 ppm, whereas those of the $N^{\delta 1}$ did so from 208 to 225 ppm (Fig. 3A, black symbols). The pattern of the ^1H–^{15}N-HMQC shows that the $N^{\varepsilon 2}$ is protonated at basic pHs [37]; the $H^{\varepsilon 1}$ and $H^{\delta 2}$ protons also titrated with a similar behavior (see below). Therefore, the His15 of unphosphorylated HPr^{sc} titrated with a $pK_a < 6.0$, as shown by the titration of the ^{15}N nuclei. We attempted to decrease the pH to obtain the acidic baseline but, at the concentrations used in the NMR experiments (300 μM), the sample precipitated [19]. To alleviate partially this problem, we carried out measurements of the titrations of the $H^{\varepsilon 1}$ and $H^{\delta 2}$ protons at 80 μM of protein concentration; sample cloudiness was observed at pHs below 4.75, but titration curves were obtained for

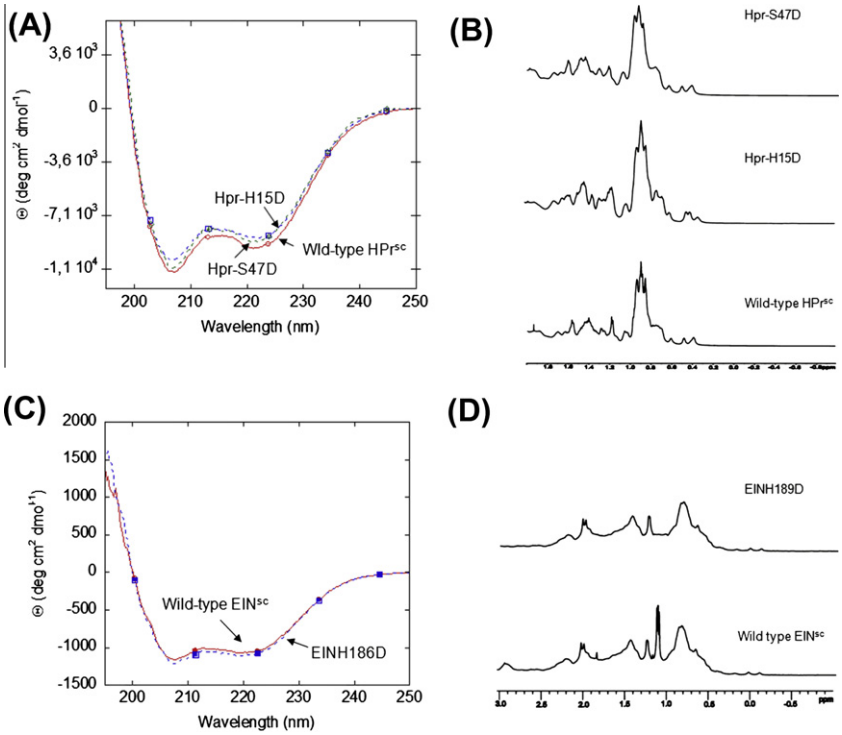

Fig. 1. Spectroscopic features and thermal stability of the phosphomimetic mutants. The (A) far-UV CD spectra, and (B) methyl regions of the ^{1}H NMR spectra of wild-type HPr^{sc} and its phosphomimetic mutants. The (C) far-UV CD spectra, and (D) methyl regions of the ^{1}H NMR spectra of wild-type EIN^{sc} and EINH186D.

Table 1
The T_ms (in °C) for the wild-type, phosphomimetic and the phosphorylated species.

Species	Far-UV CD[a]	Fluorescence[a]	DSC[b]
Wild-type HPr^{sc}	69.6 ± 0.5	69.14 ± 0.03	69
Hpr-H15D	61.5 ± 0.4	62.3 ± 0.2	64
Hpr-S47D	74.5 ± 0.7	75.5 ± 0.7	73
P∼HPr^{sc}	66.5 ± 0.6[d]	67.05 ± 0.04	c
Wild-type EIN^{sc}	60.6 ± 0.3		59.3
EINH186D	55.5 ± 0.5		57.4
P∼EIN^{sc}	54.8 ± 0.9[d]		c

[a] Errors are error fittings to Eq. (1). All the thermal denaturations, except those of the phosphorylated species, were reversible.
[b] The T_m values were obtained from deconvolution of calorimetric traces to a two-state model.
[c] Not determined due to overlapping of the calorimetric transitions of the phosphorylated and unphosphorylated species (see Fig. 4, SI).
[d] The values of the T_m are apparent due to the overlapping of the sigmoidal curves of the unphosphorylated and phosphorylated species.

both protons, which yielded an apparent pK_a of 5.5 (Fig. 2, SI). However, caution must be taken with this apparent acidic constant, since it was obtained in the presence of aggregated species of HPr^{sc} [19].

The P∼HPr^{sc} species

We could not carry out the biophysical characterization of P∼HPr^{sc} by far-UV CD due to the strong absorbance of the components of the phosphorylation buffer (see 'Protein phosphorylation'). We attempted to remove the components of the buffer by gel filtration, but the eluting HPr^{sc} species was not phosphorylated (as revealed by its NMR chemical shifts). We think that the N–P bond is so unstable, that without the components of the phosphorylation buffer, the protein reverts to the unphosphorylated species.

The fluorescence spectrum of the P∼HPr^{sc} showed a maximum at 333 nm, as that of the wild-type [19]. The methyl region of its 1D-NMR spectrum suggests that its structure is native-like; only small changes in the intensity of some methyl groups were observed (Fig. 3, SI, top). It could be thought that these variations in the NMR spectra of the P∼HPr^{sc} were due to the components of the phosphorylation buffer (see 'Protein phosphorylation'); however, it must be noted that the proteins of such buffer, which could appear at this region, are added in catalytic amounts (1 and 10 μM), and therefore would not be observable by NMR. Finally it could be suggested that the biophysical characterization of P∼HPr^{sc} is rather weak because of the absence of far-UV CD; however, the similarity of the ^{1}H 1D-NMR spectra of unphosphorylated HPr, Hpr-H15D and P∼HPr^{sc}, and the similar T_ms of Hpr-H15D and P∼HPr^{sc} (Table 1) (see below) suggest that the far-UV CD spectrum of the phosphorylated species must be similar to that of the phosphomimetic mutant.

Previous ^{15}N NMR studies of model compounds [38] suggest that a phosphorylated ^{15}N should resonate between 200 and 210 ppm. The values of the chemical shifts for N$^{\varepsilon 2}$ in P∼HPr^{sc} go from 175 (at pH 5.5) to 186 (at pH 8.5) ppm, and those for N$^{\delta 1}$ go from 190 to 220 ppm (Fig. 3A, red symbols); the chemical shifts of H$^{\varepsilon 1}$ and H$^{\delta 2}$ protons also titrated in this region with a similar behavior (data not shown). The four obtained pK_as yielded an average value of 7.5 ± 0.2, close to that expected for a solvent-exposed imidazole ring [39]. Furthermore, the pattern of signals in the ^{1}H–^{15}N-HMQC spectra suggests that the dominant neutral tautomeric form is that with the hydrogen at the N$^{\varepsilon 2}$ position (Fig. 3C) [37]. Then, we can conclude that: (a) phosphorylation in HPr^{sc} occurs at the N$^{\delta 1}$ of His15 (as suggested by the comparison of the chemical shifts with those of model compounds); (b) the pK_a of His15 increased upon phosphorylation; and (c) the chemical shifts of the N$^{\varepsilon 2}$ of the His15 did not change substantially upon phosphorylation.

As with the phosphomimetic Hpr-H15D, the stability of the P∼HPr^{sc} was lower than that of wild-type, as measured either by fluorescence or far-UV CD (Table 1). The far-UV thermograms (Fig. 2A) were noisier than those of the phosphomimetics due to the components of the phosphorylation buffer (see 'Protein phos-

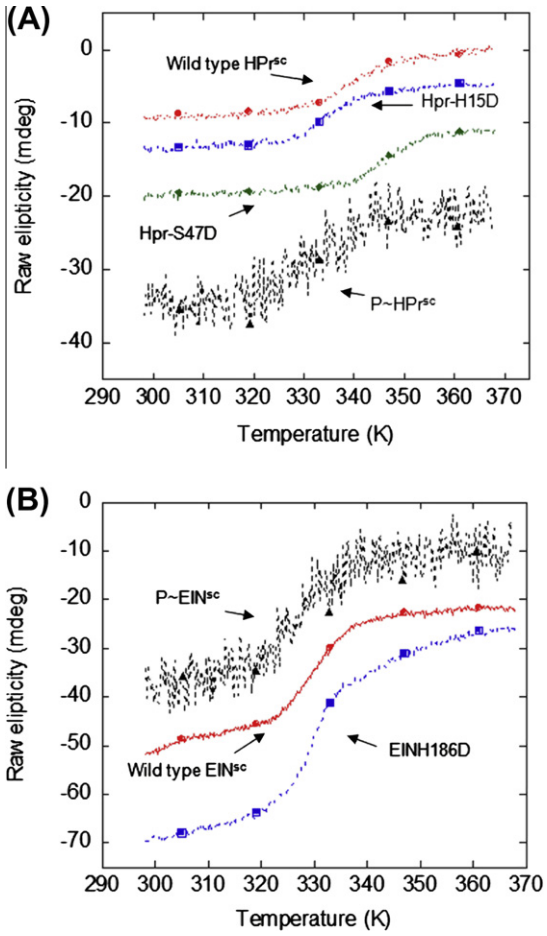

Fig. 2. Thermal denaturations as followed by far-UV CD. (A) Thermal denaturations curves of wild-type HPr^{sc} (red); Hpr-H15D (blue), Hpr-S47D (green), and P∼HPr^{sc} (black). (B) Thermal denaturations of wild-type EIN^{sc} (red), EINH186D (blue) and P∼EIN^{sc} (black). In both panels, the units in the y-axis are arbitrary to allow for an easier comparison among the thermograms, because of the similar molar ellipticity of the three proteins (see previous figure). (For interpretation of the references to color in this figure legend, the reader is referred to the web version of this article.)

phorylation'). Interestingly enough, the apparent van't Hoff enthalpy of the fluorescence thermal denaturation of P∼HPr^{sc} was smaller (39.7 kcal mol^{-1}) than that of the wild-type (65.2 kcal mol^{-1}); that is, the transition in the P∼HPr^{sc} was broader than that of wild-type, thus exhibiting lower unfolding cooperativity. Moreover, the thermal reversibility curve of P∼HPr^{sc}, followed by fluorescence, showed the same broadness (61.2 kcal mol^{-1}) and the same T_m (67.6 °C) as that of HPr^{sc}. These results suggest that the P∼HPr^{sc} is not present in the reheating scan, probably due to the low stability of the N–P bond; a similar behavior was observed in the DSC scans (see below) It is important to note that the values of T_m obtained from spectroscopic measurements for P∼HPr^{sc} will be affected by the melting of the unphosphorylated protein, whose sigmoidal curve will overlap partially with that of the P∼HPr^{sc}.

We attempted to carry out DSC experiments of P∼HPr^{sc}, but the thermogram peak corresponding to the calorimetric denaturation of HPr^{sc} overlapped with that of P∼HPr^{sc} (probably due to the low stability of the N–P bond), precluding any reliable interpretation (Fig. 4B, SI) It could be thought that the P∼HPr^{sc} could be stabilized under particular conditions; however, given the fragility of the N–P bond, and since its weakness increases with temperature, any thermal study of the phosphorylated species will detect always a population of the unphosphorylated protein.

Structural features and stability of the EIN^{sc} phosphomimetic mutant and the P∼EIN^{sc} species

Phosphomimetic mutant

The phosphomimetic mutant of EIN^{sc} (EINH186D) showed a far UV CD spectrum similar to that of wild-type EIN^{sc} (Fig. 1C), suggesting that the α + β structure was not changed in the mutant. Moreover, comparison of the ^{1}H NMR spectra in the methyl regions suggests that EINH186D is native-like (Fig. 1D).On the other hand, the thermal stability of the EINH186D was lower than that of wild-type EIN^{sc} (Table 1 and Figs. 2B and 4C of SI).

There are three histidines in EIN^{sc}, namely, His12, His21 and His186 (which is the active-site one). The ^{1}H–^{15}N-HMQC spectrum of EIN^{sc} shows three sets of signals with the hydrogen at the N$^{\varepsilon 2}$ in the neutral tautomeric form [37] (Fig. 3B). Their pK_as were in the range 7.2–7.5 (Fig. 3B).

The P∼EIN^{sc} species

We could not carry out the biophysical characterization of P∼EIN^{sc} by far-UV CD due to the strong absorbance of the components of the phosphorylation buffer (see 'Protein phosphorylation'). Comparison of the methyl regions of the 1D-NMR spectra of the phosphorylated and unphosphorylated species suggests that the structure of P∼EIN^{sc} is native-like (Fig. 1, SI, bottom), since no variations were observed. As with P∼HPr^{sc}, it could be thought that the biophysical characterization of P∼EIN^{sc} was rather weak; however, the similarity of the ^{1}H 1D-NMR spectra of unphosphorylated EIN^{sc}, EINH186D and P∼EIN^{sc}, and the similar T_ms of EINH186D and P∼EIN^{sc} (Table 1) (see below) suggest that the far-UV CD spectrum of the phosphorylated species must be similar to that of the phosphomimetic mutant.

As with EINH186D, the stability of the P∼EIN^{sc} was lower than that of wild-type EIN^{sc} (Table 1), as measured by far-UV CD. The far-UV thermograms were noisier than that of EINH186D due to the presence of the components of the phosphorylation buffer (Fig. 2B). As with the HPr species, it must be indicated that the T_m obtained from far-UV CD for the P∼EIN^{sc} was affected by the equilibrium with the unphosphorylated species (Table 1).

We attempted to carry out DSC experiments of P∼EIN^{sc}, but the peak of the calorimetric denaturation of wild-type EIN^{sc} partially overlapped with that of P∼EIN^{sc} (Fig. 4D, SI) Interestingly enough, none of the peaks observed in the heating experiments had the maximum at the temperature of unfolding of wild-type EIN^{sc}. We do not know the reasons of this behavior,but it could be due to problem baselines with the phopshorylation reaction buffer, or reversible reactions between EIN^{sc} and its components. However, the maximum of the reheating peak (∼58 °C) was close to the T_m determined from spectroscopic measurements for wild-type EIN^{sc} (Table 1), suggesting that the reheating experiment only contained non-phosphorylated protein.

The ^{1}H–^{15}N-HMQC spectrum of P∼EIN^{sc} only showed two sets of signals (the signal with red filled symbols in Fig. 3B disappeared). The observed signals did not show any variation in the chemical shifts at the different pHs, when compared to those measured in the spectrum of the unphosphorylated species (Fig. 3B). The most plausible explanation to these findings is that the signals of the N$^{\varepsilon 2}$ and N$^{\delta 1}$ of His186 become too broad during the titration of P∼EIN^{sc}. Similar broadening of the imidazole signals have been observed in hydrogen-bonded histidine rings in other proteins [32].

Binding of the phosphomimetic and phosphorylated species

We determined the affinity of wild-type HPr^{sc} and the phosphomimetics (Hpr-H15D, Hpr-S47D) for EIN^{sc} and its phosphomimetic (EINH186D), by using ITC (Fig. 4). The K_D of the EIN^{sc}–HPr^{sc} complex is 12 μM; the K_Ds of EIN^{sc}–Hpr-H15D and

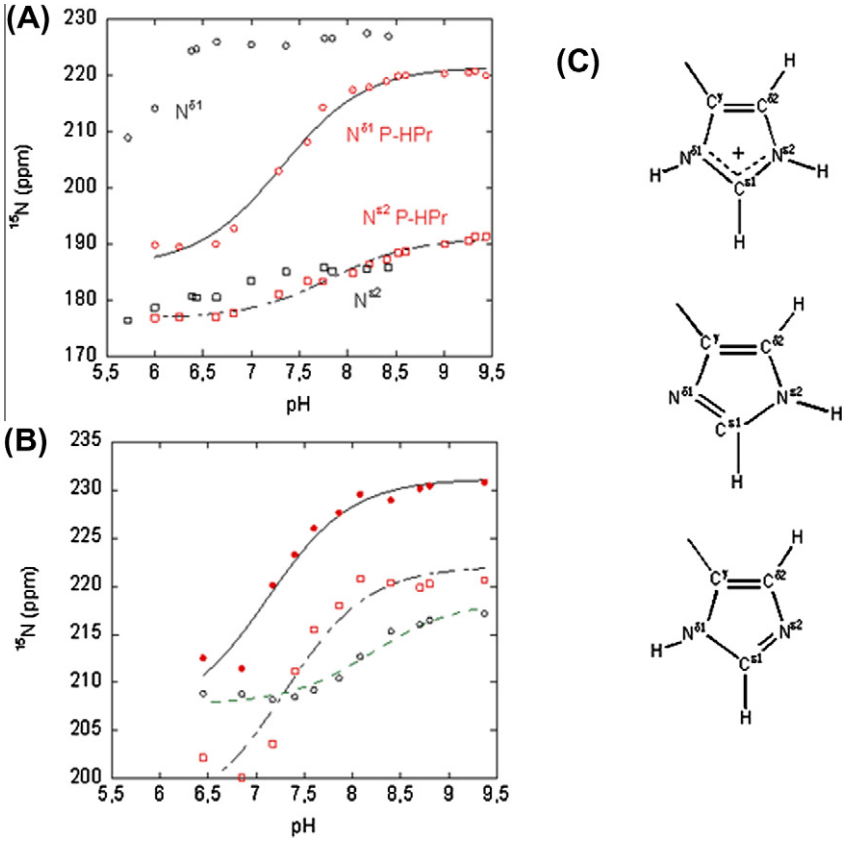

Fig. 3. Titration of the histidine residues in the HPr^{sc} species and in unphosphorylated EIN^{sc}. (A) Titration of the N$^{\varepsilon2}$, N$^{\delta1}$ of unphosphorylated HPr^{sc} (black) and P∼HPr^{sc} (red). (B) Titration of the N$^{\varepsilon2}$ of the three histidines in unphosphorylated wild-type EIN^{sc}. The lines through the data are the fitting to the Henderson–Hasselbalch equation (Eq. (4)). (C) The different tautomeric species of the histidine aromatic ring: (top) the acidic species with both N$^{\varepsilon2}$ and N$^{\delta1}$ protonated; (middle) the basic N$^{\varepsilon2}$ protonated species; and (bottom) the basic N$^{\delta1}$ protonated species. (For interpretation of the references to color in this figure legend, the reader is referred to the web version of this article.)

EINH186D–Hpr-H15D complexes were two- and three-times higher, respectively; the K_D of EINH186D–HPr^{sc} complex was within the same range as that of the complex formed by the wild-type species of both proteins; and the K_Ds of EIN^{sc}–Hpr-S47D and EINH186D–Hpr-S47D complexes were three- to two-times smaller than that of EIN^{sc}–HPr^{sc} complex, respectively. Finally, the K_D of the biphosphorylated complex (P∼EIN^{sc}–P∼HPr^{sc}) was 13-times higher than that of the unphosphorylated one (Table 2). The value of ΔS was positive for all complexes suggesting that binding reactions were entropically driven; this result indicates a main favorable contribution from hydrophobic desolvation in the binding reaction.

To determine the buffer-independent enthalpy of the binding reaction (ΔH^0), the effect of the buffer ionization heat was taken into account by carrying out the binding reaction in two buffers: Tris and Mops, which have different ionization enthalpies (11.7 and 5.5 kcal mol^{-1}, respectively). With this procedure [40], the ΔH^0 and the number of exchanged protons, n_H, between the complex and the bulk solution were obtained (Table 2). A positive value of n_H indicates a protonation by the complex (such as in EIN^{sc}–HPr^{sc} complex, where the n_H is close to 0.5); on the other hand, a negative value of n_H indicates a deprotonation.

Discussion

Stability of the phosphomimetic mutants and phosphorylated species

Knowledge of the phosphorylation effects on the protein structure and energetics allows us to understand biochemical pathways. In general terms, protein phosphorylation can result in [41]: (a) no changes in protein structure; (b) modifying the conformation of loops or residues, towards a binding-competent structure; (c) changing protein surface; (d) altering the electrostatics of a region without conformational changes; and, (e) causing allosterism. From our thermodynamic studies, we can conclude that there are small conformational changes in HPr^{sc} and EIN^{sc} upon phosphorylation. Furthermore, based on the agreement between the T_ms from spectroscopic measurements of the corresponding phosphomimetic and phosphorylated species (Table 2), and the similarity of the ^{1}H 1D-NMR spectra, we suggest that mutants mimic properly the stability of the phosphorylated proteins.

A similar decrease in the stability of H15E ad H15A mutants, when compared to the unphosphorylated wild-type, has been also observed in HPr^{ec} [42]. From our modeled structure of wild-type HPr^{sc} [25], His15 is located at the N terminus of the first helical region, acting as an N-cap. Since there is a net positive charge at the N-terminal region of the α-helix [25], a negative charge (such as that provided by the phosphate and the aspartate) should stabilize the protein. In unphosphorylated HPr^{ec}, the N$^{\varepsilon2}$-proton is strongly hydrogen-bonded. Based in: (i) the absence of large changes in the chemical shifts of N$^{\varepsilon2}$ in unphosphorylated species (Fig. 3A, black symbols); and, (ii) the pK_a < 6.0 for the unphosphorylated His15, we suggest that the N$^{\varepsilon2}$ of unphosphorylated HPr^{sc} is also hydrogen-bonded. This hydrogen-bond would be disrupted in the P∼HPr^{sc}, as judged from the changes in the chemical shifts (Fig. 3A, red symbols); furthermore, this hydrogen-bond would not be present in the Hpr-H15D, and hence, its lower stability when compared to that of wild-type.

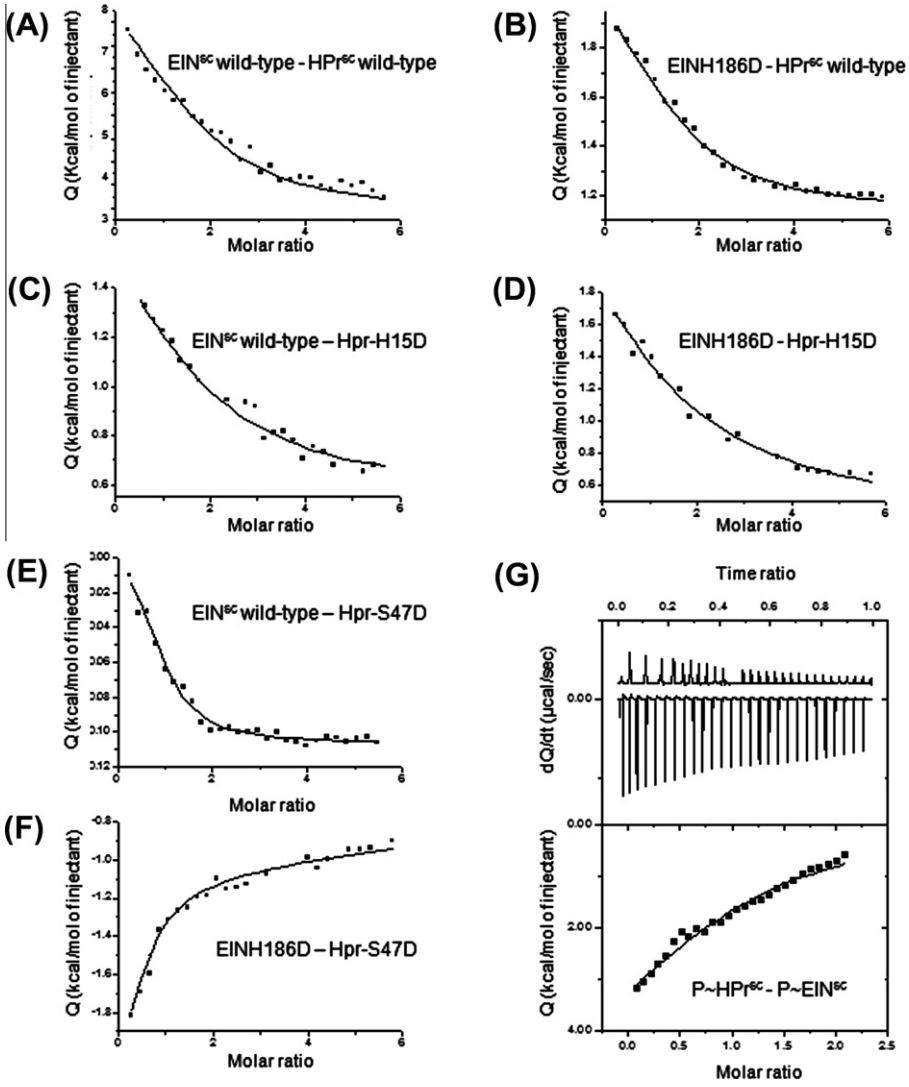

Fig. 4. Binding between the phosphomimetic mutants and the phosphorylated forms of EIN^{sc} and HPr^{sc} as monitored by ITC. Binding curve for the titration between /EIN^{sc}–HPr^{sc} (A); EINH186D–HPr^{sc} (B); EIN^{sc}–Hpr-H15D (C); EINH186D–Hpr-H15D (D); EIN^{sc}–Hpr-S47D (E); EINH186D–Hpr-S47D (F); and P∼EIN^{sc}–P∼HPr^{sc} (G). In (G) the raw data (top) and control experiment with P∼HPr^{sc} (bottom) are shown.

The Hpr-S47D was more stable than the wild-type protein, as it has been observed in other phosphomimetics of HPr^{ec} [41] and HPr^{bs} [43]. From our HPr^{sc} modeled structure [25], Ser47 is at the N-cap of the short second helix, and therefore, the stabilization caused for this mutation can be easily explained as due to an electrostatic interaction between the negatively charged residue and the helix macrodipole [44].

A similar decrease in the stability of EIN phosphomimetics has been observed in alanine and glutamate mutations in EIN^{ec} [45]. In our modeled structure of wild-type EIN^{sc} [22], His186 is located at the N terminus of the sixth α-helix. Thus, as it has been observed for His189 in unphosphorylated EIN^{ec} (with a pK_a of 6.3) [13], we should expect a low pK_a for the active-site histidine of EIN^{sc}. However, none of the three histidines observed in unphosphorylated EIN^{sc} showed a titration midpoint lower than 7.0 (Fig. 3B); furthermore, the three imidazoles in unphosphorylated EIN^{sc} had the proton at the N$^{\varepsilon 2}$ position at basic pHs, as shown by the pattern of signals in the HMQC spectra. Upon phosphorylation, one set of signals disappeared, whereas the other two showed the same pK_as as those in the unphosphorylated species. In unphosphorylated EIN^{sc}, the rate of proton exchange relative to the chemical shift difference (for the charged and neutral species) allows the observation of the imidazole resonances over the pH titration; conversely, in P∼EIN^{sc}, that rate leads to line broadening and disappearance of the resonances of the active-site histidine in the NMR spectra. This difference in the exchange rate is probably the result of conformational changes around the active-site upon phosphorylation; interestingly enough, a similar disappearance of the imidazole signals during titration has been observed in the His15 of P∼HPr^{ec} [46], and in other proteins where the imidazoles are hydrogen-bonded [32]. The breaking of hydrogen-bonds, based on the different titration behavior of the imidazole nitrogens in both EIN^{ec} species [13,45,47], explains the lower stability of the EIN^{ec} phosphomimetics. However, in the absence of structural information on the active-site histidine of EIN^{sc} in both states, we can only speculate on the presence of a hydrogen-bond, which could be disrupted upon phosphorylation, decreasing the stability of the mutant.

Impact of the phosphorylation on the stability of the EIN^{sc}–HPr^{sc} complexes: biological implications

The binding processes among the different HPr^{sc} and EIN^{sc} species were always entropically driven. This is the opposite to our results in the binding of intact wild-type EI^{sc} to HPr^{sc}, which was

Table 2
Thermodynamic parameters for the interactions of the phosphomimetic, phosphorylated and the wild-type species.

Complex[a]	K_D (μM)	ΔH^0 (kcal/mol)[b]	ΔG^0 (kcal/mol)[c]	$-T\Delta S^0$ (kcal/mol K)[d]	n_H[e]
EIN^{sc}–HPr^{sc}	12	−2.9	−6.7	−3.81	0.52
EIN^{sc}–Hpr-H15D	23	5.80	−6.3	−12.1	−0.33
EIN^{sc}–Hpr-S47D	3.5	0.36	−7.4	−7.8	−0.02
EINH186D–HPr^{sc}	10	0.85	−6.8	−7.6	−0.03
EINH186D–Hpr-H15D	32	6.02	−6.1	−12.1	−0.34
EINH186D–Hpr-S47D	6	−1.6	−7.1	−5.43	0.09
P∼EIN^{sc}–P∼HPr^{sc}	132	f	−5.3	f	f

[a] All titrations were carried out in 10 mM Tris or Mops buffers (pH 7.0) at 25 °C. K_D is the dissociation constant. Relative errors in binding enthalpy and dissociation constant are 10% and 20%, respectively. Relative errors in binding Gibbs energy and entropy are 2% and 10%, respectively.
[b] The value of the buffer-independent enthalpy for the binding reaction, determined by carrying out experiments in 10 mM Tris and Mops buffers (pH 7.0) at 25 °C, by using Eq. (3).
[c] The ΔG^0 is the binding free energy at 25 °C, determined as $\Delta G^0 = RT\ln K_D$.
[d] The value of the entropy of the binding reaction at 25 °C, determined as $-T\Delta S^0 = \Delta G^0 - \Delta H^0$.
[e] The number of exchanged protons, determined by carrying out experiments in 10 mM Tris and Mops buffers (pH 7.0) at 25 °C, by using Eq. (3).
[f] Not determined.

enthalpically driven [23]; furthermore, the affinity of intact wild-type EI^{sc} for HPr^{sc} is smaller (∼100 μM) than that measured (∼10 μM) for other PTS proteins [23, and references therein] and for EIN^{sc} (this work). We suggest that the difference in the K_Ds must rely on structural effects. Comparison of the K_D of EIN^{sc}–HPr^{sc}, with that of EIN^{ec}–HPr^{ec} [45,48] suggests that the large differences must be due to the presence of the EIC^{sc}. This region promotes dimerization and binding to PEP, and it would not be surprising that, due to the solution conditions (which affect EI dimerization [49]), the energetics of EIC^{sc} dimerization was very different to that of others EIC. These differences in the dimerization of EIC^{sc} could also explain the change from an enthalpy- to an entropy-driven binding reaction; since HPr binding requires previous dissociation of the EI dimer, the enthalpy of the reaction would contain a contribution from the EI dissociation.

The apparent binding enthalpies, $\Delta H_{meas;buffer}$, show a large degree of variation among the binding reactions (data not shown). Although these differences might reflect conformational changes upon binding, as suggested when comparing to similar studies of phosphomimetics in *E. coli* [45,48], however, it must be taken into account that the measured binding enthalpy by ITC will contain a contribution from buffer ionization (protonation or deprotonation) if there is a net proton exchange between the complex and the bulk solution. This net exchange is caused by a pK_a change upon binding in certain ionizable groups elicited by a change in their solvation microenvironment. For that reason, the buffer-independent enthalpy (ΔH^0 in Table 2) must be calculated from a set of experiments performed at the same conditions using buffers with different ionization enthalpies. Reporting either the buffer-dependent or the buffer-independent binding enthalpy may lead to discrepancies when comparing different binding interactions among the HPrs from several species. The measured n_H values in this work suggest that the binding is slightly different among the different phosphorylated species assayed, regarding the proton exchange coupled to binding, since it varies among the complexes. It is interesting to note that the n_H measured for the wild-type species is similar to that obtained for EI^{sc}–HPr^{sc} (0.72) [23].

The proposed structural changes occurring upon binding must be small and located close to the active-site residues, as concluded from the structure of the EIN^{ec}–HPr^{ec} complex [14] and the sequence similarity among the PTS proteins in *E. coli* and *S. coelicolor* [16–18], and they might contribute slightly to the observed enthalpy differences. However, as mentioned before, differences in the protonation signature will also contribute significantly to the overall binding enthalpy. In addition, these conformational changes will be accompanied by two major competing entropic contributions: (a) an unfavorable conformational entropy loss (due to binding); and, (b) a favorable desolvation entropy gain. These two entropic terms, together with the roto-translational entropy loss characteristic of any binding process, give rise to the highly favorable entropic contribution to the Gibbs energy of the binding reactions (Table 2).

In *S. coelicolor* the complex with the largest affinity is EIN^{sc}–Hpr-S47D. Mutations at this serine (or its equivalent in other HPr species) affect the PEP dependent-EI catalyzed phosphorylation at His15, varying the K_m of the EI-HPr phosphorylation reaction, and lowering the phosphoryl carrier activity of HPr [2, and references therein]. Although, at the best of our knowledge, there are not measurements *in vitro* of the affinity between EIN and (P∼Ser)HPr in the literature, the differences in the catalytic parameters have been explained as due to the proximity between the Glu84 in EIN^{ec} and the negatively charged phosphorylated serine when the complex is formed [14], therefore decreasing the affinity of the complex, and varying the K_m. This electrostatic repulsion seems to be screened in the EIN^{sc}–Hpr-S47D complex, suggesting that there must be other structural, non-electrostatic features behind the variations in the enzymatic parameters governing the phosphorylation reaction of the (P∼Ser)HPr.

The weakest affinities occurred for the phosphomimetics (or alternatively, for the phosphorylated species). The large K_D can be attributed to the unfavorable (positive) binding enthalpy (which could be only determined in the binding of the phosphomimetics, Table 2). Electrostatic repulsion between the active-site phosphorylated histidines must be responsible for the decreased affinity; we think that the affinity is smaller for the phosphorylated species than for the phosphomimetics due to the larger size of phosphorylated histidines, when compared to aspartates.

Conclusions

We have shown that the stabilities of the phosphorylated species of HPr^{sc} and EIN^{sc} are lower than those of the unphosphorylated counterparts, due to local conformational changes. Binding of the different EIN^{sc} and HPr^{sc} species causes small local, active-site conformational rearrangements. Furthermore, the binding among the different un- or phosphorylated species is always entropically driven, a thermodynamic profile opposite to that of the interaction of full-length EI^{sc} with HPr^{sc}, suggesting that the dimerization of the EIC^{sc} is important in determining the affinity and the enthalpy of binding of the intact EI^{sc} with HPr^{sc}.

Acknowledgments

We thank Prof. Paul F. Fitzpatrick for handling the manuscript; we thank both reviewers for helpful suggestions and discussions. We thank Fritz Titgemeyer for the kindly gift of EI^{sc} and HPr^{sc}

genes. We deeply thank May García, María del Carmen Fuster, Javier Casanova and Raquel Jorquera for technical assistance. The stays of RD in the laboratory of AVC were supported by the Spanish Ministerio de Ciencia e Innovación (BFU2008-02302-BMC). We thank Dr. David Reguera for allowing the short stays of RD in the laboratory of A.V.C., under the help of the Grant FIS2010-10522-E.

This work was supported by the Spanish Ministerio de Ciencia e Innovación (MCINN) (CTQ2011-24393, CSD2008-00005 to J.L.N., and BFU2010-19451 to AVC), Diputación General de Aragón (PI044/09 to A.V.C.), and intramural BIFI 2011 projects (to A.V.C. and J.L.N.). A.I.M.G. was recipient of a fellowship of the MCINN (FBI). SMR was supported by the Andalusia government.

The funding sources have no involvement in the research described. The authors declare they do not have any competing interest. R.D., A.I.M.G., D.A.L., A.V.C. and J.L.N. carried out the experiments; R.D., A.V.C. and J.L.N. analyzed the data; S.M.R. and J.M.C.J. provided material and strains; A.V.C. and J.L.N. designed the experiments and wrote the manuscript.

Appendix A. Supplementary data

Supplementary data associated with this article can be found, in the online version, at http://dx.doi.org/10.1016/j.abb.2012.07.004.

References

[1] B. Görke, J. Stülke, Nat. Microbiol. 6 (2008) 613–624.
[2] J. Deutscher, C. Francke, P.W. Postma, Microbiol. Mol. Biol. Rev. 70 (2006) 939–1031.
[3] J. Deutscher, Curr. Opin. Microbiol. 11 (2008) 87–93.
[4] J.W. Lengeller, K. Jahreis, Contrib. Microbiol. 16 (2009) 65–87.
[5] M. Weigel, M.A. Kukuruzinska, A. Nakazawa, E.B. Waygood, S. Roseman, J. Biol. Chem. 257 (1982) 14477–14491.
[6] K.Y. Hu, M.H. Jr Saier, Res. Microbiol. 153 (2002) 405–415.
[7] E.B. Waygood, N.D. Meadow, S. Roseman, Anal. Biochem. 95 (1979) 293–304.
[8] M.A. Kukuruzinska, B.W. Turner, G.K. Ackers, S. Roseman, J. Biol. Chem. 259 (1984) 11679–11681.
[9] B.R. Lee, P. Lecchi, L. Panell, H. Jaffe, A. Peterkofsky, Arch. Biochem. Biophys. 312 (1994) 121–124.
[10] P.P. Zhu, R.H. Szczepanowski, N.J. Nosworthy, A. Ginsburg, A. Peterkofsky, Biochemistry 38 (1999) 15470–15479.
[11] S.J. Brokx, J. Talbot, F. Geroges, E.B. Waygood, Biochemistry 39 (2000) 3624–3635.
[12] D.I. Liao, E. Silverton, Y.J. Seok, B.R. Lee, A. Peterkofsky, D.R. Davies, Structure 4 (1996) 861–872.
[13] D.S. Garrett, Y.K. Seok, D.I. Liao, A. Peterkofsky, A.M. Gronenborn, G.M. Clore, Biochemistry 36 (1997) 2517–2530.
[14] D.S. Garrett, Y.K. Seok, A. Peterkofsky, A.M. Gronenborn, G.M. Clore, Nat. Struct. Biol. 6 (1999) 166–173.
[15] A. Teplyakov, K. Lim, P.-P. Zhu, G. Kapadia, C.C.H. Chen, J. Schwartz, A. Howard, P.T. Reddy, A. Peterkofsky, O. Herzberg, Proc. Natl. Acad. Sci. USA 103 (2006) 16218–16223.
[16] S. Parche, R. Schmid, F. Titgemeyer, Eur. J. Biochem. 265 (1999) 308–317.
[17] H. Nothaft, D. Dresel, A. Willimek, K. Mahr, M. Niederweis, F. Titgemeyer, J. Bacteriol. 185 (2003) 7019–7023.
[18] H. Nothaft, S. Parche, A. Kamionka, F. Titgemeyer, J. Bacteriol. 85 (2003) 929–937.
[19] G. Fernández-Ballester, J. Maya, A. Martin, S. Parche, J. Gómez, F. Titgemeyer, J.L. Neira, Eur. J. Biochem. 270 (2003) 2254–2267.
[20] J.L. Neira, J. Gómez, Eur. J. Biochem. 271 (2004) 2165–2181.
[21] E. Hurtado-Gómez, F.N. Barrera, J.L. Neira, Biophys. Chem. 115 (2–3) (2005) 229–233.
[22] E. Hurtado-Gómez, G. Fernández-Ballester, H. Nothaft, J. Gómez, F. Titgemeyer, J.L. Neira, Biophys. J. 90 (2006) 4592–4604.
[23] E. Hurtado-Gómez, O. Abián, F.J. Muñoz, M.J. Hernáiz, A. Velázquez-Campoy, J.L. Neira, Biophys. J. 95 (2008) 1336–1348.
[24] F. Chauvin, A. Fomenkov, C.R. Johnson, S. Roseman, Proc. Natl. Acad. Sci. USA 93 (1996) 7028–7031.
[25] J.A. Poveda, G. Fernández-Ballester, M. Prieto, J.L. Neira, Biochemistry 46 (2007) 7252–7260.
[26] B. Miroux, J.E. Walker, J. Mol. Biol. 260 (1996) 289–298.
[27] M. Romero-Beviar, S. Martínez-Rodríguez, J. Prieto, E. Goormaghtigh, U. Ariz, M.L. Martínez-Chantar, J. Gómez, J.L. Neira, Prot. Eng. Design Select. 23 (2010) 729–742.
[28] L.A. Alcaraz, M. del Alamo, F.N. Barrera, M.G. Mateu, J.L. Neira, Biophys. J. 93 (2007) 1264–1276.
[29] S.C. Gill, P.H. von Hippel, Anal. Biochem. 182 (1989) 319–326.
[30] S. Benjwal, S. Verma, K.-H. Röhm, O. Gursky, Protein Sci. 15 (2006) 635–639.
[31] M. Piotto, V. Saudek, V. Sklenar, J. Biomol. NMR 2 (1992) 661–665.
[32] N. Doucet, G. Khirich, E.L. Kovrigin, J.P. Loria, Biochemistry 50 (2011) 1723–1730.
[33] A. Bax, M. Ikura, L.E. Kay, D.A. Torchia, R. Tschudin, J. Magn. Reson. 86 (1990) 304–318.
[34] D. Marion, M. Ikura, R. Tschudin, A. Bax, J. Magn. Reson. 85 (1989) 393–399.
[35] D.S. Wishart, C.G. Bigam, J. Yao, F. Abildgaard, H.J. Dyson, E. Oldfield, J.L. Markley, B.D. Sykes, J. Biomol. NMR 6 (1995) 135–140.
[36] K. Wüthrich, NMR of Proteins and Nucleic Acids, Wiley, New York, 1986.
[37] J.G. Pelton, D.A. Torchia, N.D. Meadow, S. Roseman, Protein Sci. 2 (1993) 543–558.
[38] A.A. Van Dijk, L.C.M. Lange, W.W. Bachovchin, G.T. Robillard, Biochemistry 29 (1990) 8164–8171.
[39] R.L. Thurlkill, G.R. Grimsley, J.M. Scholtz, C.N. Pace, Protein Sci. 15 (2006) 1214–1218.
[40] J. Gómez, E. Freire, J. Mol. Biol. 252 (1995) 337–350.
[41] L.N. Johnson, D. Barford, Annu. Rev. Biophys. Biomol. Struct. 22 (1993) 199–232.
[42] M.E. Huffine, J.M. Scholtz, J. Biol. Chem. 271 (1996) 28898–28902.
[43] K. Pullen, P. Rajagopal, B.R. Branchini, M.E. Huffine, J. Reizer, M.H. Saier Jr., J.M. Scholtz, R.E. Klevit, Protein Sci. 4 (1995) 2478–2486.
[44] W.G.J. Hol, P.Th. Van Duijnen, H.J.C. Berendsen, Nature 273 (1978) 443–446.
[45] A. Ginsburg, R.H. Szczepanowski, S.B. Ruvinov, N.J. Nosworthy, M. Sondej, T.C. Umland, A. Peterkofsky, Protein Sci. 9 (2000) 1085–1094.
[46] N.A.J. Van Nuland, R. Boelens, R.M. Scheek, G.T. Robillard, J. Mol. Biol. 246 (1995) 180–193.
[47] D.S. Garret, Y.J. Seok, A. Peterkofsky, G.M. Clore, A.M. Gronenborn, Protein Sci. 7 (1998) 789–793.
[48] J.Y. Suh, M. Cai, G.M. Clore, J. Biol. Chem. 283 (2008) 18980–18989.
[49] H.V. Patel, K.A. Vyas, R. Savtchenko, S. Roseman, J. Biol. Chem. 281 (2006) 17570–17578.